Introduction

Heterobimetallic active sites have been discovered in a number of proteins that carry out life-sustaining chemical transformations, including [NiFe] hydrogenase, the heme a_3/Cu_B site in cytochrome *c* oxidase, Cu/Zn superoxide dismutase, the Fe/Mn site in class 1c of the ribonucleotide reductases (R2c)[1,2] and R2-like ligand binding oxidase (R2lox).[34,5] The biosynthetic assembly pathways for heterobimetallic cofactors[6] have piqued the interest of biochemists and synthetic chemists alike, as they highlight an important debate regarding how metalation in biology is controlled.[7–11] Despite having distinctly different redox potentials, Fe^{II} and Mn^{II} often function interchangeably in biology. Enzymes, such as epimerases,[12] superoxide dismutases,[13] and extradiol dioxygenases,[14,15] can execute cellular functions with either Fe or Mn. Similarly, three classes of ribonucleotide reductases, featuring diiron (class 1a), dimanganese (class 1b), and iron/manganese (class 1c) active sites have been discovered.[9,16–18] Despite sharing nearly identical coordination environments (Figure 1A), the FeFe, MnMn, and FeMn sites are assembled *in vivo* with distinct metal specificity.

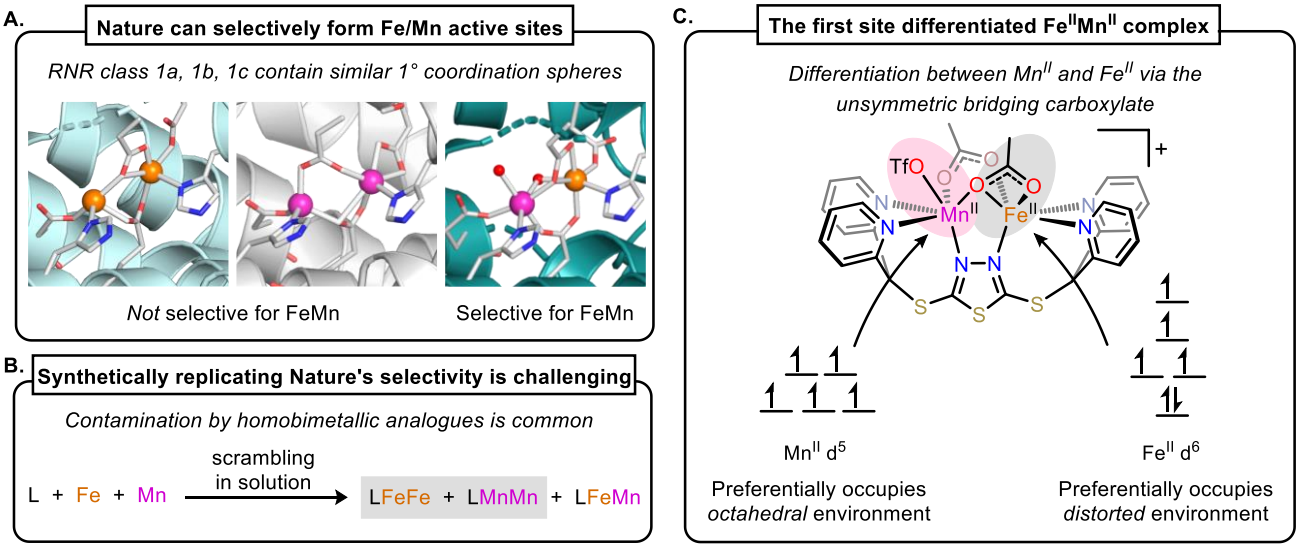

Figure 1. (A) Pymol rendered active sites of ribonucleotide reductase class 1a, left (PDB: 1PIY), 1b, middle (PDB: 6TQW), and 1c, right (PDB: 4M1I). (B) Scrambling of heterobimetallic complexes to form homobimetallic complexes. (C) Site-differentiated $Fe^{II}Mn^{II}$ complex examined in this work.

The existence of FeMn heterobimetallic cofactors within R2c and R2lox enzymes is intriguing, as these enzymes selectively coordinate Fe^{II} ion at one site and Mn^{II} ion at the other. Both Fe^{II} and Mn^{II} ions bind to biological/non-biological ligands weakly and tend to prefer similar coordination geometries.[6] Typically, proteins that utilize metals with lower binding affinities or lower intracellular concentrations employ metal-specific transporters in order to achieve correct metallation.[19–21] However, no such metallochaperones have been identified for manganese. In fact, the assembly of FeMn cofactors directly contradicts the divalent metal binding rules ($Mn^{II} < Fe^{II}$) outlined in the Irving-Williams series.[22]

The remarkable FeMn heterobimetallic specificity displayed by R2c and R2lox has been the subject of intense scrutinization through metalation study of apoproteins[4,5,23–26] and synthetic model systems.[27–31] Currently, no synthetic model can reproduce R2c and R2lox's FeMn selectivity, leading to the hypothesis that precisely crafted three-dimensional protein environments are required to overcome the thermodynamic barriers that govern divalent metal binding ($Mn^{II} < Fe^{II}$). However, the specific structural motif that enables Mn^{II} selectivity over Fe^{II} remain unclear. While synthetic models in theory could provide answers regarding the selectivity of metal binding, preparation of heterobimetallic $Fe^{II}Mn^{II}$ complexes is challenging.[29,32] The few examples of $Fe^{II}Mn^{II}$ complexes in the literature require sequential addition of Fe^{II} and Mn^{II} sources[32–34] - a highly different condition comparing to the *in vitro* and *in vivo* assembly of R2c and R2lox, where both Fe^{II} and Mn^{II} are present during protein folding. Additionally, synthetic heterobimetallic FeMn complexes often scramble to afford the corresponding homobimetallic FeFe and MnMn analogues, further complicating the quantitative analysis (Figure 1B).[29,32]

Herein, we report the synthesis of a site-differentiated $Fe^{II}Mn^{II}$ complex supported by Py_4DMcT ligand (**L**, Figure 1C), along with its homometallic diiron and tetramanganese analogues. Similar to R2lox and R2c, the ligand **L** selectively bind one Fe^{II} and one Mn^{II} in the presence of equimolar amount of Fe^{II} and Mn^{II} source, regardless of the order of Fe^{II} and Mn^{II} addition. Diffraction Anomalous Fine Structure (DAFS) analysis shows our $Fe^{II}Mn^{II}$ model complex has the same selectivity as R2lox, with Fe^{II} ion selectively occupies the distorted site created by unsymmetrically coordinated carboxylate (Figure 1C). The structural similarities of our $Fe^{II}Mn^{II}$ model complex to the active site of R2lox and R2c along with its precise FeMn selectivity allows us to propose a new mechanism for heterobimetallic formation that does not contradict the classical Irving-Williams series.

Results and discussion

Synthesis and characterization. Inspired by previous work from our group,[35,36] we attached four pyridines to a bis-mercaptan-1,3,4-thiadiazole linker to form the new 2-((di(pyridin-2-yl)methyl)thio)-5-((pyridin-2-yl(pyridin-3-yl)methyl)thio)-1,3,4-thiadiazole ligand (Py_4DMcT, **L**, Figure 2). Reaction of the dipotassium salt of dimercapto-1,3,4-thiadiazol with a slight excess of dipyridylchloromethane under ambient conditions in methanol leads to Py_4DMcT formation in 85% yield (Scheme 1).

Following the successful synthesis of Py_4DMcT, we first set out to investigate whether it could support a bimetallic diiron complex. Sequential treatment of Py_4DMcT with one equivalent each of bis-acetonitrile iron(II) triflate ($Fe^{II}(OTf)_2MeCN_2$) and iron(II) acetate ($Fe^{II}(OAc)_2$) in a 1:1 chloroform/methanol solution, followed by slow diffusion of diethyl ether affords bright orange crystals in 70% yield. Single-crystal X-ray diffraction (XRD) of the orange crystals reveals the diiron complex [**L**Fe^{II}_2(MeOH)$(OAc)_2$]$(OTf)_2$ (Figure SX). The coordinated MeOH can be removed by recrystallization of crude [**L**Fe^{II}_2(MeOH)$(OAc)_2$]$(OTf)_2$ from dichloromethane with slow diffusion of diethyl ether, with similar yield. Single-crystal XRD analysis of the resulting crystals shows that the coordinated methanol solvent molecule is replaced by an inner-sphere triflate anion as [**L**$Fe^{II}_2$$(OAc)_2$(OTf)][OTf] (**$Fe^{II}Fe^{II}$-OTf**) (Scheme 1, right). Notably, in both structures, the diiron core features one bridging acetate anion coordinated in a symmetric, μ-1,3 binding mode, and the other in an unsymmetric μ-1,1 binding mode (Figure 2A).

Scheme 1. Synthesis of Py_4DMcT (**L**) and metal complexes.

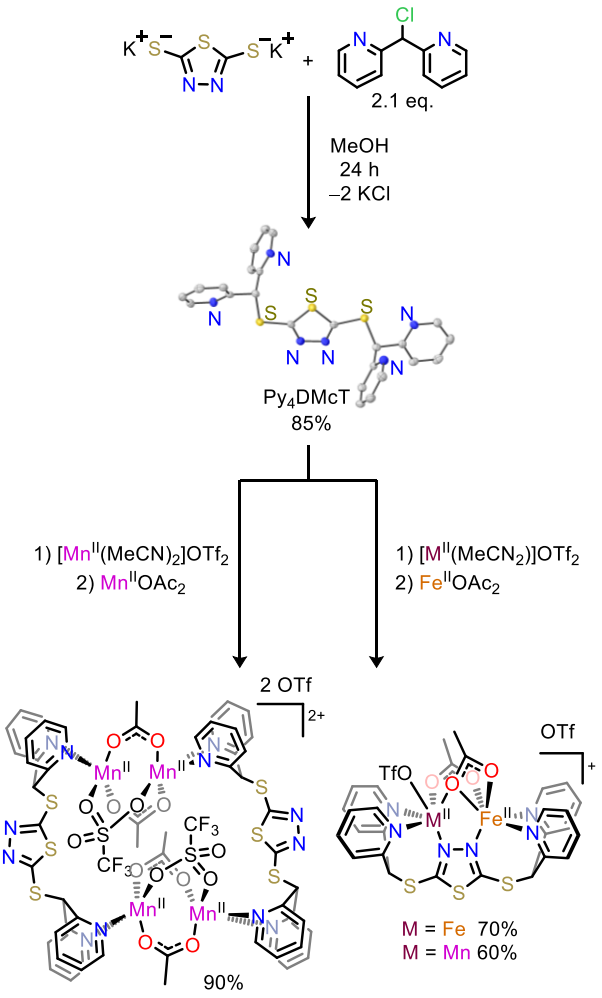

With the successful isolation of the diiron species, we turned towards the isolation of the heterobimetallic iron/manganese analogue. Py_4DMcT was treated with one equivalent of bis-

acetonitrile manganese(II) triflate ($Mn^{II}(OTf)_2MeCN_2$), followed by one equivalent of $Fe^{II}(OAc)_2$. Slow diffusion of diethyl ether into a dichloromethane solution resulted in the isolation of yellow crystals of [**L**$Fe^{II}Mn^{II}(OAc)_2(OTf)$][OTf] **$Fe^{II}Mn^{II}$-OTf** in 60% yield.

Similar to **$Fe^{II}Fe^{II}$-OTf** complex, **$Fe^{II}Mn^{II}$-OTf** crystallizes in the *$P2_1/c$* space group but with different unit cell parameters. Single-crystal XRD analysis reveals two metal centers (Mn or Fe) bridged by two carboxylate ligands, one in a μ-1,3 binding mode and the other in a μ-1,1 binding mode. The M-M separation is 3.479 Å, compared to 3.464 Å in **$Fe^{II}Fe^{II}$-OTf** and 3.65 Å and 3.2 Å in R2lox and R2c, respectively.[37,38] We tentatively assigned the metal center at the distorted octahedral site as Fe^{II}, due to the better agreement of such a model with the electron density map (R^2 = 4.30% vs. 4.46% with a reversed Fe/Mn assignment). The core of our complexes closely resembles the unsymmetric core of R2lox in its reduced $Fe^{II}Mn^{II}$ state, where the central thiadiazole moiety acts as a model for the third bridging μ-1,3 carboxylate presents in R2lox. The unsymmetric coordinated carboxylate ligand with the μ-1,1 binding mode (E227 in Ct R2c and E202 GkR2lox) is a conserved feature across the superfamily of bacterial multicomponent monoxygenases (BMMs),[39–42] and is the only feature in the primary coordination spheres of R2c and R2lox that differentiates the Fe^{II} site from the Mn^{II} site.

The heterobimetallic identity of **$Fe^{II}Mn^{II}$-OTf** was further confirmed by spectroscopic analysis. The UV-vis spectrum of **$Fe^{II}Mn^{II}$-OTf** is similar to that of **$Fe^{II}Fe^{II}$-OTf** (Figure 2D) but with roughly half of the intensity. This observation is similar to previous results of FeFe and FeMn complexes reported by Lu, et al., in which the difference in molar extinction coefficients was attributed to the presence of one iron center versus two.[32] The ^{1}H NMR spectrum of **$Fe^{II}Mn^{II}$-OTf** reveals nine broad resonances from -30 ppm to 140 ppm that are distinct from the six paramagnetic peaks of **$Fe^{II}Fe^{II}$-OTf** (Figure 2C). Additional ^{1}H-NMR resonances were observed for **$Fe^{II}Mn^{II}$-**

OTf than **$Fe^{II}Fe^{II}$-OTf**, consistent with the unsymmetric nature of **$Fe^{II}Mn^{II}$-OTf**.[28] Mossbauer spectroscopic analysis also revealed distinct differences between the two compounds (Figure 2E, 2F). Namely, the best fit for the Mossbauer spectrum of **$Fe^{II}Fe^{II}$-OTf** employs two iron sites, whereas for **$Fe^{II}Mn^{II}$-OTf**, one iron site leads to the best fit.

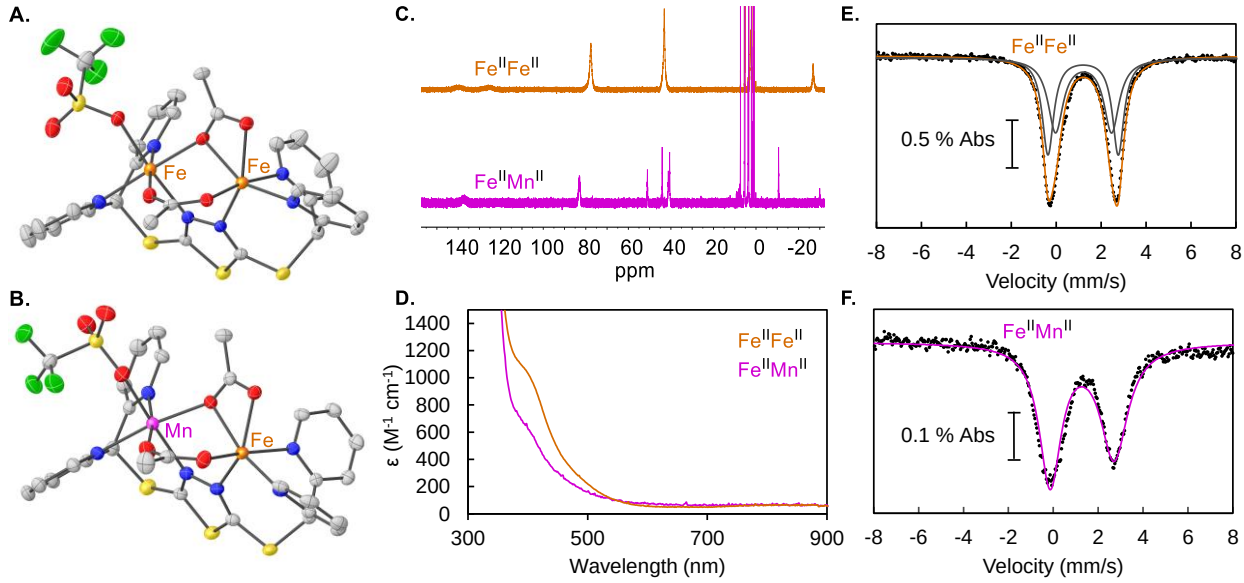

Figure 2. Solid-state structures of (A) $Fe^{II}Fe^{II}$-OTf, and (B) $Fe^{II}Mn^{II}$-OTf with thermal ellipsoids shown at 50% level of probability. Outer sphere counter anions, co-crystallized solvents and minor components of disorder are omitted for clarity. (C) ^{1}H-NMR spectra of $Fe^{II}Fe^{II}$-OTf (top) and $Fe^{II}Mn^{II}$-OTf (bottom), 2.5 mM in CD_2Cl_2. (D) UV-vis of $Fe^{II}Fe^{II}$-OTf and $Fe^{II}Mn^{II}$-Otf, 2.5 mM in CH_2Cl_2, (E) Solid-state Mössbauer spectrum of $Fe^{II}Fe^{II}$-OTf. (F) Solid-state Mössbauer spectrum of $Fe^{II}Mn^{II}$-OTf.

After isolation and characterization of **$Fe^{II}Fe^{II}$-OTf** and **$Fe^{II}Mn^{II}$-OTf**, we attempted to complete the series of bimetallic complexes by preparing the analogous dimanganese species. However, treatment of **L** with $Mn(OAc)_2$ and $Mn(OTf)_2$ resulted in the isolation of a colorless tetramanganese paddlewheel complex, **Mn^{II}_4-OTf** (Scheme 1, bottom). **Mn^{II}_4-OTf** is ^{1}H NMR silent due to fast relaxation caused by the Mn^{II} center.[43,44] XRD analysis revealed two dimanganese sites sandwiched between two Py_4DMcT ligands. All manganese ions are symmetrically bridged by two acetate anions and one triflate anion with an Mn-Mn distance of 3.860 Å. The formation of the tetramanganese complex, rather than a dimanganese species, suggests that **L** is unable to accommodate two Mn centers in the same environment as **$Fe^{II}Mn^{II}$-OTf** and **$Fe^{II}Fe^{II}$-OTf**. This

observation is consistent with the minimal $Mn^{II}Mn^{II}$ cofactor formation observed in R2lox.[4,5,23,26,37]

Mechanism of selective heterobimetallic formation Two distinct mechanisms have been proposed for the selective metalation of FeMn cofactors in R2c and R2lox (Scheme 2).[23] Apo-R2c first loads two Mn^{II} ions at both sites A and B, followed by the replacement of one Mn^{II} with Fe^{II}, preferentially at site B (Scheme 2 left). Conversely, R2lox first coordinates an Fe^{II} ion at the distorted site B. The successful loading of Fe^{II} triggers the binding of the second metal, which is predominantly Mn^{II} (ca. 50% - 80 % selectivity, depending on relative Fe^{II}/Mn^{II} concentration, Scheme 2 right). Thus, both R2c and R2lox have seemingly tuned their binding sites to coordinate Mn^{II} and Fe^{II} with similar affinities.[23] Although there have been attempts to synthetically replicate this selective assembly of heterobimetallic Fe/Mn sites, these studies are largely complicated by significant contamination from the homobimetallic FeFe and MnMn analogues due to scrambling in the reaction solution.[29,45] In contrast, the successful isolation of a pure $Fe^{II}Mn^{II}$ complex in our case suggests that unlike previous synthetic complexes, a selective assembly mechanism could be at play.

Scheme 2. Heterobimetallic assembly in R2c and R2lox

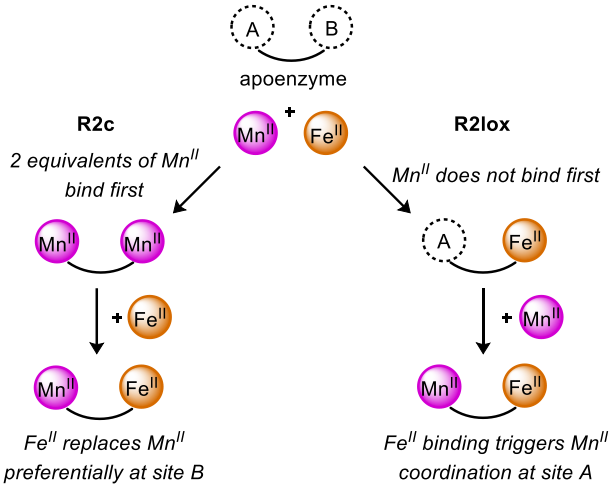

To begin our examination of the assembly route of **$Fe^{II}Mn^{II}$-OTf**, we sought to determine whether the order of addition of metal salts affects the yield of the heterobimetallic species. If the yield of the heterobimetallic species depended on the order of metal salt addition, this would be sufficient evidence to determine that heterobimetallic assembly was due to the synthetic procedure,

rather than an intrinsic property of the ligand itself. We performed an in-situ ^{1}H-NMR study by varying the order of addition of $M^{II}(OTf)_2(MeCN)_2$ and $M^{II}(OAc)_2$ (M = Mn or Fe) to **L**. The ligand was treated with the first metal salt for 15 minutes with stirring before the second metal salt was added. The product of the reaction was extracted into dichloromethane-d_2 and analyzed with quantitative ^{1}H NMR. Although **Mn^{II}_4-OTf** is ^{1}H NMR silence, the concentration of both **$Fe^{II}Fe^{II}$-OTf** and **$Fe^{II}Mn^{II}$-OTf** can be determined based on independent ^{1}H NMR calibration curves.

The results of quantitative ^{1}H NMR analysis of the four reactions are summarized in Table 1. In all cases, **$Fe^{II}Mn^{II}$-OTf** was formed preferentially in 74-77% yield, regardless of the order of addition of the metal salts. Further, the amount of contamination of the corresponding **$Fe^{II}Fe^{II}$-OTf** species was quite low (ca. 6%), which is comparable to the FeMn selectivity displayed by metalation of apo-R2c and apo-R2lox. If the ligand **L** did not discriminate between Fe^{II} and Mn^{II}, much higher amounts of **$Fe^{II}Fe^{II}$-OTf** would be expected, along with lower (< 50%) amounts of **$Fe^{II}Mn^{II}$-OTf**.[29,32] From this information, we concluded that regardless of the order of addition of the metal, the formation of **$Fe^{II}Mn^{II}$-OTf** in all four cases occur via the same assembly route, leading us to develop two potential hypotheses for the observed FeMn heterobimetallic selectivity.

Table 1. ^{1}H-NMR yields of Fe^{II}_2-OTf and $Fe^{II}Mn^{II}$-OTf under various conditions

Order of addition of metal salts	Yield of **Fe^{II} Fe^{II}**	Yield of **$Fe^{II}Mn^{II}$**
(1) $[Fe^{II}(MeCN_2)](OTf)_2$ *(2)* $Mn^{II}(OAc)_2$	6.6%	77.0%
(1) $[Mn^{II}(MeCN_2)](OTf)_2$ *(2)* $Fe^{II}(OAc)_2$	5.8%	75.4%
(1) $Fe^{II}(OAc)_2$ (2) $[Mn^{II}(MeCN_2)](OTf)_2$	5.8%	73.8%
(1) $Mn^{II}(OAc)_2$ *(2)* $[Fe^{II}(MeCN_2)](OTf)_2$	6.6%	77.0%

The first explanation involves the availability of Fe^{II} and Mn^{II}, which has been proposed as the main reason FeMn cofactors form in Nature.[8,17] Although Fe^{II} and Mn^{II} coexist in biology in similar concentrations, the binding of Fe^{II} is expected to be thermodynamically more favorable

than that of Mn^{II}, according to the Irving-Williams series. In our case, we reason that **L** would not violate Irving-Williams due to the lack of secondary or tertiary structure that compels a high Mn^{II} specificity. Therefore, it is reasonable to assume that Fe^{II} would coordinate first to **L**, creating an Fe^{II}-deficient environment. By default, Mn^{II} coordination occurs second to form the final FeMn species. The successful assembly of our FeMn complex, therefore, depends on a low "availability" of Fe^{II} (one equivalent per **L**). In order for the effective assembly of the FeMn species to occur, most of the Fe^{II} ions must be consumed in the first step to ensure selective binding of Mn^{II} as the second metal.

To verify our "Fe^{II} first, Mn^{II} second" hypothesis, we subjected **L** to a series of reactions with increasing "metal availability". However, the ratio of Fe^{II} : Mn^{II} remains 1:1. We employed the triflate salts of Fe^{II} and Mn^{II} along with TBA(OAc) as acetate source, so as not to bias acetate coordination to any metals prior to the assembly of the bimetallic complexes. In all reactions, $Fe^{II}(OTf)_2(MeCN)_2$ and $Mn^{II}(OTf)_2(MeCN)_2$ were pre-mixed before the addition to **L** and TBAOAc was added after **L** and the metals were stirred for 15 minutes**.** After TBAOAc addition, the mixture was stirred for 20 more minutes before an aliquot of the reaction was taken, dried, and redissolved in CD_2Cl_2 and analyzed by ^1H NMR. The results of these reactions are summarized in Table 2.

Table 2. ^1H NMR yield of **$Fe^{II}Mn^{II}$-OTf** as a function of the ratio of Fe^{II} : Mn^{II} : L

Reaction	**Ratio of Fe^{II} : Mn^{II} : L**	Yield of **$Fe^{II}Mn^{II}$-OTf**
A	2 : 2 : 1	0 %
B	1.75 : 1.75 : 1	49.0 %
C	1.50 : 1.50 : 1	72.0 %
D	1.25 : 1.25 : 1	75.0 %
E	1 : 1 : 1	80.0 %

Consistent with the "Fe^{II} first, Mn^{II} second" hypothesis, the yield of heterobimetallic **$Fe^{II}Mn^{II}$-OTf** complex decreases as the metal availability increase from one equivalent per **L** to two equivalents per **L**. The most striking result is that when two equivalents of Fe^{II} and Mn^{II} ions are available, the metal specificity is completely reversed with no **$Fe^{II}Mn^{II}$-OTf** formation, further

implying that the formation of the heterobimetallic species is only favored under Fe^{II}-deficient conditions. With two equivalents of Fe^{II} present, Fe^{II} binding outcompetes that of Mn^{II}, which is in agreement with the divalent metal binding rules outlined in the Irving-Williams series.[22] The high specificity for **$Fe^{II}Fe^{II}$-OTf** under excess amount of Fe^{II} and Mn^{II} is different from metal preference of R2lox. *In vitro* metalation of apo-R2lox with excess amount of Fe^{II} and Mn^{II} sources performed by Högbom et al. shows the formation of 50:50 mixture of FeFe and FeMn site. The favorable coordination of Fe^{II} over Mn^{II} is also observed in biological environments, and has led researchers to suggest that many Mn-containing proteins may simply be metalated "by default" when an organism accumulates high amounts of Mn.[46,47]

Furthermore, we observed an even greater yield of $Fe^{II}Mn^{II}$-OTf (ca. 80%) when Fe^{II}/Mn^{II}/**L** are mixed in a 1 : 1 : 1 ratio before the addition of two equivalents of TBA(OAc). It is likely that coordination of two equivalents of OAc to $[\mathbf{L}Fe]^{2+}$ organizes the second octahedral binding pockets that facilitates facile binding of either Fe^{II} or Mn^{II} as the second metal. This hypothesis is consistent with the observations of Shafaat et al. that (a) binding of two metals is ordered and (b) Mn^{II} cannot productively binds if the Fe^{II} site is unoccupied.

To provide further quantitative evidence for the "Fe^{II} first, Mn^{II} second" hypothesis, we investigated the equilibrium between the monometallic iron and manganese complexes via ^{1}H NMR. ^{1}H NMR analysis of a mixture of **L** with different equivalent of $Fe^{II}TFSI_2$ suggests that **L** forms monometallic complexes with Fe^{II} in the absence of acetate. We were unable to confirm the formation of mono-Mn complex $[\mathbf{L}Mn^{II}]TFSI_2$ from a mixture of **L** with $Mn^{II}TFSI_2$, since $[\mathbf{L}Mn^{II}]TFSI_2$ is NMR silent. Given the monometallic $[\mathbf{L}Fe^{II}]TFSI_2$ complex shows well resolved paramagnetic resonances, while $[\mathbf{L}Mn^{II}]TFSI_2$ complex is NMR silent, comparison of the ^{1}H NMR spectra $[\mathbf{L}Fe^{II}]TFSI_2$ in the presence of various equivalents of $Mn^{II}TFSI_2$ allows us to calculate an

equilibrium constant K_{eq} = [**L**Fe^{II}]$^{2+}$/[**L**Mn^{II}]$^{2+}$ = 2.38, suggesting a mild preference for binding Fe^{II} first. Assuming (a) the binding the first metal is thermodynamically controlled and (b) no selectivity for the binding of the second metal, the amount of correctly assembled **$Fe^{II}Mn^{II}$-OTf** expected is 70%. Our observed yields of 74-77% were slightly higher than expected, pushing us to consider additional mechanisms for FeMn heterobimetallic selectivity.

Scheme 3. Assembly of heterobimetallic $Fe^{II}Mn^{II}$ complex

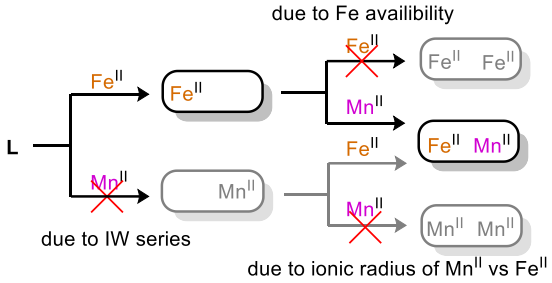

The second potential reason to explain the higher than expected yields of FeMn heterobimetallic complex is the inability of **L** to accommodate two Mn^{II} centers in close proximity. As shown by the tetrametallic solid-state structure of the Mn^{II} complex, the ligand **L** cannot accommodate the same bimetallic MnMn structure as observed in the case of **$Fe^{II}Mn^{II}$-OTf** and **$Fe^{II}Fe^{II}$-OTf** . The bias of **L** against the bimetallic MnMn species could be explained by the marginally larger size of Mn^{II} versus Fe^{II}.

Summary and Conclusions

In summary, we have reported a series of synthetic model complexes, **$Fe^{II}Fe^{II}$-OTf**, **$Fe^{II}Mn^{II}$-OTf**, and **Mn^{II}_4-OTf**, which have shed valuable light onto the mechanism of FeMn heterobimetallic assembly in Nature. In contrast to the formation of the bimetallic **$Fe^{II}Fe^{II}$-OTf** and **$Fe^{II}Mn^{II}$-OTf** complexes, ligand **L** cannot accommodate a dinuclear $Mn^{II}Mn^{II}$ structure, suggesting that **L** can discern the subtle differences between the smaller Fe^{II} and larger Mn^{II} ions. The inability of **L** to incorporate two Mn^{II} ions in a dinuclear geometry is consistent with the apparent lack of MnMn cofactor formation in R2lox. The single crystal X-ray analysis of $Fe^{II}Fe^{II}$-OTf and $Fe^{II}Mn^{II}$-OTf display a bimetallic core containing an unsymmetrically bridged carboxylate ligand, which allows for the differentiation between the two sites. This feature allows

for site-differentiation and selective binding of Fe^{II} at the distorted site. The site-differentiating carboxylate is a feature shared by both R2lox and R2c at the reduced state, therefore likely the critical factor that allows us to reproduce the unique FeMn metal specificity.

Importantly, treatment of **L** with one equivalent each of Fe^{II} and Mn^{II} resulted in selective assembly of **$Fe^{II}Mn^{II}$-OTf** up to 80% yield. Such selectivity requires an iron-deficient environment – similar metalation experiments with equimolar, but excess amounts, of Fe^{II} and Mn^{II} leads to inversed metal specificity with the formation of **$Fe^{II}Fe^{II}$-OTf**. This observation is consistent with the hypothesis that the intracellular availability of metal ions plays a role in metal selection. Overall, our metal binding studies reveal that the successful assembly of **$Fe^{II}Mn^{II}$-OTf** originates from the selective binding of Fe^{II} as the first metal, creating an Fe-deficient/Mn-rich environment that promotes selective loading of Mn^{II} as the second metal. Our study suggests that assembly of an $Fe^{II}Mn^{II}$ heterobimetallic site can still be accomplished without violating the classic Irving-Williams theory. In fact, the strong thermodynamic preference for Fe^{II} over Mn^{II} is the driving force for correct heterobimetallic assembly, although the overall results of the reaction appear to be contrary to the Irving-Williams theory. Our model study provides an alternative explanation for the long-standing puzzle of why R2lox and R2c appear to be violating the fundamental thermodynamic rules governing coordination chemistry. In fact, R2lox and R2c can be correctly assembled via proper design of the primary coordination sphere and favorable (iron deficient) assembly conditions. We expect site-differentiation not only promotes the correct assembly of the FeMn site, but also has implications towards oxidative reactivity. Additionally, many questions remain as to why the selectivity of FeMn in R2lox is enriched in the presence of O_2, considering FeFe-R2lox reacts with O_2 faster than the FeMn cofactor. These intriguing questions will be the subject of future studies.

References

(1) Jiang, W.; Yun, D.; Saleh, L.; Barr, E. W.; Xing, G.; Hoffart, L. M.; Maslak, M. A.; Krebs, C.; Bollinger, J. M. A Manganese(IV)/Iron(III) Cofactor in Chlamydia Trachomatis Ribonucleotide Reductase. *Science (80-.).* **2007**, *316*, 1188–1191.

(2) Jiang, W.; Yun, D.; Saleh, L.; Martin Bollinger, J.; Krebs, C. Formation and Function of the Manganese(Iv)/Iron(Iii) Cofactor in Chlamydia Trachomatis Ribonucleotide Reductase. *Biochemistry*. American Chemical Society December 30, 2008, pp 13736–13744.

(3) Andersson, C. S.; Högbom, M. A Mycobacterium Tuberculosis Ligand-Binding Mn/Fe Protein Reveals a New Cofactor in a Remodeled R2-Protein Scaffold. *Proc. Natl. Acad. Sci.* **2009**, *106*, 5633–5638.

(4) Griese, J. J.; Roos, K.; Cox, N.; Shafaat, H. S.; Branca, R. M. M.; Lehtiö, J.; Gräslund, A.; Lubitz, W.; Siegbahn, P. E. M.; Högbom, M. Direct Observation of Structurally Encoded Metal Discrimination and Ether Bond Formation in a Heterodinuclear Metalloprotein. *Proc. Natl. Acad. Sci.* **2013**, *110*, 17189–17194.

(5) Shafaat, H. S.; Griese, J. J.; Pantazis, D. A.; Roos, K.; Andersson, C. S.; Popović-Bijelić, A.; Gräslund, A.; Siegbahn, P. E. M.; Neese, F.; Lubitz, W.; Högbom, M.; Cox, N. Electronic Structural Flexibility of Heterobimetallic Mn/Fe Cofactors: R2lox and R2c Proteins. *J. Am. Chem. Soc.* **2014**, *136*, 13399–13409.

(6) Högbom, M. The Manganese/Iron-Carboxylate Proteins: What Is What, Where Are They, and What Can the Sequences Tell Us? *JBIC J. Biol. Inorg. Chem. 2009 153* **2009**, *15*, 339–349.

(7) Griese, J. J.; Srinivas, V.; Högbom, M. Assembly of Nonheme Mn/Fe Active Sites in Heterodinuclear Metalloproteins. *J. Biol. Inorg. Chem.* **2014**, *19*, 759–774.

(8) Cotruvo, J. A.; Stubbe, J. Metallation and Mismetallation of Iron and Manganese Proteins in Vitro and in Vivo: The Class I Ribonucleotide Reductases as a Case Study. *Metallomics* **2012**, *4*, 1020–1036.

(9) Högbom, M. Metal Use in Ribonucleotide Reductase R2, Di-Iron, Di-Manganese and Heterodinuclear—an Intricate Bioinorganic Workaround to Use Different Metals for the Same Reaction. *Metallomics* **2011**, *3*, 110–120.

(10) Bosch, S.; Comba, P.; Gahan, L. R.; Hanson, G. R.; Noble, C.; Schenk, G.; Wadepohl, H. Selective Coordination of Gallium(III), Zinc(II), and Copper(II) by an Asymmetric Dinucleating Ligand: A Model for Metallophosphatases. *Chem. – A Eur. J.* **2015**, *21*, 18269–18279.

(11) Bosch, S.; Comba, P.; Gahan, L. R.; Schenk, G. Asymmetric Mono- and Dinuclear GaIII and ZnII Complexes as Models for Purple Acid Phosphatases. *J. Inorg. Biochem.* **2016**, *162*, 343–355.

(12) Sobota, J. M.; Imlay, J. A. Iron Enzyme Ribulose-5-Phosphate 3-Epimerase in <Em>Escherichia Coli</Em> Is Rapidly Damaged by Hydrogen Peroxide but Can Be Protected by Manganese. *Proc. Natl. Acad. Sci.* **2011**, *108*, 5402 LP – 5407.

(13) Beyer Jr, W. F.; Fridovich, I. In Vivo Competition between Iron and Manganese for Occupancy of the Active Site Region of the Manganese-Superoxide Dismutase of Escherichia Coli. *J. Biol. Chem.* **1991**, *266*, 303–308.

(14) Lipscomb, J. D. Mechanism of Extradiol Aromatic Ring-Cleaving Dioxygenases. *Curr. Opin. Struct. Biol.* **2008**, *18*, 644–649.

(15) Vaillancourt, F. H.; Bolin, J. T.; Eltis, L. D. The Ins and Outs of Ring-Cleaving Dioxygenases. *Crit. Rev. Biochem. Mol. Biol.* **2006**, *41*, 241–267.

(16) Nordlund, P.; Reichard, P. Ribonucleotide Reductases. *Annu. Rev. Biochem.* **2006**, *75*, 681–706.

(17) Huang, M.; Parker, M. J.; Stubbe, J. Choosing the Right Metal: Case Studies of Class I Ribonucleotide Reductases. *J. Biol. Chem.* **2014**, *289*, 28104.

(18) Kutin, Y.; Srinivas, V.; Fritz, M.; Kositzki, R.; Shafaat, H. S.; Birrell, J.; Bill, E.; Haumann, M.; Lubitz, W.; Högbom, M.; Griese, J. J.; Cox, N. Divergent Assembly Mechanisms of the Manganese/Iron Cofactors in R2lox and R2c Proteins. *J. Inorg. Biochem.* **2016**, *162*, 164–177.

(19) Pufahl, R. A.; Singer, C. P.; Peariso, K. L.; Lin, S. J.; Schmidt, P. J.; Fahrni, C. J.; Cizewski Culotta, V.; Penner-Hahn, J. E.; O'Halloran, T. V. Metal Ion Chaperone Function of the Soluble Cu(I) Receptor Atx1. *Science (80-.).* **1997**, *278*, 853–856.

(20) Rae, T. D.; Schmidt, P. J.; Pufahl, R. A.; Culotta, V. C.; O'Halloran, T. V. Undetectable Intracellular Free Copper: The Requirement of a Copper Chaperone for Superoxide Dismutase. *Science* **1999**, *284*, 805–808.

(21) Vickery, L. E.; Cupp-Vickery, J. R. Molecular Chaperones HscA/Ssq1 and HscB/Jac1 and Their Roles in Iron-Sulfur Protein Maturation. *http://dx.doi.org.proxy.lib.ohio-state.edu/10.1080/10409230701322298* **2008**, *42*, 95–111.

(22) Irving, H.; Williams, R. J. P. 637. The Stability of Transition-Metal Complexes. *J. Chem. Soc.* **1953**, *3245*, 3192–3210.

(23) Kutin, Y.; Srinivas, V.; Fritz, M.; Kositzki, R.; Shafaat, H. S.; Birrell, J.; Bill, E.; Haumann, M.; Lubitz, W.; Högbom, M.; Griese, J. J.; Cox, N. Divergent Assembly Mechanisms of the Manganese/Iron Cofactors in R2lox and R2c Proteins. *J. Inorg. Biochem.* **2016**, *162*, 164–177.

(24) Miller, E. K.; Trivelas, N. E.; Maugeri, P. T.; Blaesi, E. J.; Shafaat, H. S. Time-Resolved Investigations of Heterobimetallic Cofactor Assembly in R2lox Reveal Distinct Mn/Fe Intermediates. *Biochemistry* **2017**, *56*, 3369–3379.

(25) Maugeri, P. T.; Griese, J. J.; Branca, R. M.; Miller, E. K.; Smith, Z. R.; Eirich, J.; Högbom, M.; Shafaat, H. S. Driving Protein Conformational Changes with Light: Photoinduced Structural Rearrangement in a Heterobimetallic Oxidase. *J. Am. Chem. Soc.* **2018**, *140*, 1471–1480.

(26) Kisgeropoulos, E. C.; Griese, J. J.; Smith, Z. R.; Branca, R. M. M.; Schneider, C. R.; Högbom, M.; Shafaat, H. S. Key Structural Motifs Balance Metal Binding and Oxidative Reactivity in a Heterobimetallic Mn/Fe Protein. *J. Am. Chem. Soc.* **2020**, *142*, 5338–5354.

(27) Sano, Y.; Lau, N.; Weitz, A. C.; Ziller, J. W.; Hendrich, M. P.; Borovik, A. S. Models for Unsymmetrical Active Sites in Metalloproteins: Structural, Redox, and Magnetic Properties of Bimetallic Complexes with MII-(μ-OH)-FeIII Cores. *Inorg. Chem.* **2017**, *56*, 14118–14128.

(28) Kerber, W. D.; Goheen, J. T.; Perez, K. A.; Siegler, M. A. Enhanced Stability of the FeII/MnII State in a Synthetic Model of Heterobimetallic Cofactor Assembly. *Inorg.*

Chem. **2015**, *55*, 848–857.

(29) Carboni, M.; Clémancey, M.; Molton, F.; Pécaut, J.; Lebrun, C.; Dubois, L.; Blondin, G.; Latour, J.-M. Biologically Relevant Heterodinuclear Iron–Manganese Complexes. *Inorg. Chem.* **2012**, *51*, 10447–10460.

(30) Carboni, M.; Latour, J. M. Enzymes with an Heterodinuclear Iron-Manganese Active Site: Curiosity or Necessity? *Coordination Chemistry Reviews*. Elsevier B.V. January 1, 2011, pp 186–202.

(31) Das, B.; Daver, H.; Singh, A.; Singh, R.; Haukka, M.; Demeshko, S.; Meyer, F.; Lisensky, G.; Jarenmark, M.; Himo, F.; Nordlander, E. A Heterobimetallic FeIIIMnII Complex of an Unsymmetrical Dinucleating Ligand: A Structural and Functional Model Complex for the Active Site of Purple Acid Phosphatase of Sweet Potato. *Eur. J. Inorg. Chem.* **2014**, *2014*, 2204–2212.

(32) Tereniak, S. J.; Carlson, R. K.; Clouston, L. J.; Victor G. Young, J.; Bill, E.; Maurice, R.; Chen, Y.-S.; Kim, H. J.; Gagliardi, L.; Lu, C. C. Role of the Metal in the Bonding and Properties of Bimetallic Complexes Involving Manganese, Iron, and Cobalt. *J. Am. Chem. Soc.* **2013**, *136*, 1842–1855.

(33) Bossek, U.; Weyhermüller, T.; Wieghardt, K.; Bonvoisin, J.; Girerd, J. J. Synthesis, e.s.r. Spectrum and Magnetic Properties of a Heterobinuclear Complex Containing the {FeIII(μ-O)(μ-MeCO2) 2MnIII}2+ Core. *J. Chem. Soc. Chem. Commun.* **1989**, No. 10, 633–636.

(34) Crossland, P. M.; Guo, Y.; Lawrence Que, J. Spontaneous Formation of an Fe/Mn Diamond Core: Models for the Fe/Mn Sites in Class 1c Ribonucleotide Reductases. *Inorg.*

Chem. **2021**, *60*, 8710–8721.

(35) Tao, W.; Bower, J. K.; Moore, C. E.; Zhang, S. Dicopper M-oxo, M-nitrosyl Complex from the Activation of NO or Nitrite at a Dicopper Center. *J. Am. Chem. Soc.* **2019**, *141*, 10159–10164.

(36) Li/Chemical-Science, R.; Tuttle, M. R.; Walter, C.; Brackman, E.; Moore, C.; Espe, M.; Rasik, C.; Adams, P.; Zhang, S.; Tuttle, M. R.; Walter, † Christopher; Brackman, E.; Moore, C. E.; Espe, M.; Rasik, C.; Adams, P.; Zhang, S. Redox-Active Zinc Thiolates for Low-Cost Rechargeable Aqueous Zn-Ion Batteries. *Chem. Sci.* **2021**.

(37) Griese, J. J.; Kositzki, R.; Schrapers, P.; Branca, R. M. M.; Nordström, X. A.; Lehtiö, J.; Haumann, M.; Högbom, X. M. Structural Basis for Oxygen Activation at a Heterodinuclear Manganese/Iron Cofactor. *J. Biol. Chem.* **2015**, *290*, 25254–25272.

(38) Dassama, L. M. K.; Krebs, C.; J. Martin Bollinger, J.; Rosenzweig, A. C.; Boal, A. K. Structural Basis for Assembly of the MnIV/FeIII Cofactor in the Class Ic Ribonucleotide Reductase from Chlamydia Trachomatis. *Biochemistry* **2013**, *52*, 6424–6436.

(39) Rosenzweig, A. C.; Frederlckt, C. A.; Lippard, S. J.; Nordlund, P. Crystal Structure of a Bacterial Non-Haem Iron Hydroxylase That Catalyses the Biological Oxidation of Methane. **1993**.

(40) Rosenzweig, A. C.; Lippard, S. J. Determining the Structure of a Hydroxylase Enzyme That Catalyzes the Conversion of Methane to Methanol in Methanotrophic Bacteria. *Acc. Chem. Res* **1994**, *27*, 229–236.

(41) Rosenzweig, A. C.; Nordlund, P.; Takahara, P. M.; Frederick, C. A.; Lippard, S. J.

Geometry of the Soluble Methane Monooxygenase Catalytic Diiron Center in Two Oxidation States. *Chem. Biol.* **1995**, *2*, 409–418.

(42) Whittington, D. A.; Lippard, S. J. Crystal Structures of the Soluble Methane Monooxygenase Hydroxylase from Methylococcus Capsulatus (Bath) Demonstrating Geometrical Variability at the Dinuclear Iron Active Site. *J. Am. Chem. Soc.* **2001**, *123*, 827–838.

(43) Bertini, I.; Turano, P.; Vila, A. J. Nuclear Magnetic Resonance of Paramagnetic Metalloproteins. *Chem. Rev.* **2002**, *93*, 2833–2932.

(44) Bertini: NMR of paramagnetic molecules in biological systems - Google Scholar https://scholar.google.com/scholar_lookup?hl=en&publication_year=1986&author=I.+Bertini&author=C.+Luchinat&title=NMR+of+Paramagnetic+Molecules+in+Biological+Systems (accessed Nov 12, 2021).

(45) Tereniak, S. J.; Carlson, R. K.; Clouston, L. J.; Young, V. G.; Bill, E.; Rémi, §; Maurice, R.; Chen, Y.-S.; Kim, H. J.; Gagliardi, L.; Lu, C. C. Role of the Metal in the Bonding and Properties of Bimetallic Complexes Involving Manganese, Iron, and Cobalt. *J. Am. Chem. Soc* **2014**, *136*, 1842–1855.

(46) Wang, J.; Capdevila, D. A.; Giedroc, D. P. Metal Ion Homeostasis. *Compr. Coord. Chem. III* **2021**, 929–953.

(47) Martin, J. E.; Lisher, J. P.; Winkler, M. E.; Giedroc, D. P. Perturbation of Manganese Metabolism Disrupts Cell Division in Streptococcus Pneumoniae. *Mol. Microbiol.* **2017**, *104*, 334–348.